Coronagraphic focal-plane wave-front estimation for exoplanet detection: application to the apodized Roddier & Roddier coronagraph

B. Paul[a,b,c],J.-F. Sauvage[a,c], L. M. Mugnier[a,c], M. N'Diaye[b,c], K. Dohlen[b,c], M. Ferrari[b,c],T. Fusco[a,c]

[a]ONERA, BP 72, 92322 Chatillon France,
[b]Laboratoire d'Astrophysique de Marseille (LAM), Université Aix-Marseille/CNRS, 13388 Marseille Cedex 13, France,
[c]Groupement d'intérêt scientifique PHASE (Partenariat Haute résolution Angulaire Sol et Espace) between Onera, Observatoire de Paris, CNRS and Université Diderot

ABSTRACT

The final performance of current and future instruments dedicated to exoplanet detection and characterisation (such as SPHERE on the VLT, GPI on Gemini North or EPICS on E-ELT) is limited by intensity residuals in the scientific image plane, which originate in uncorrected optical aberrations. After correction of the atmospheric turbulence, the main contribution to these residuals are the quasi-static aberrations introduced upstream of the coronagraphic mask. In order to reach the final detectivity, these aberrations have to be estimated and compensated for. Some of these aberrations are not seen by the wave-front sensor of the AO loop but only by the scientific instruments.
In order to measure and compensate for these aberrations, we have recently proposed a dedicated focal-plane sensor called COFFEE (for COronagraphic Focal-plane wave-Front Estimation for Exoplanet detection), based on an analytical model for coronagraphic imaging. In this communication, we first present a thorough characterisation of COFFEE's performance, by means of numerical simulations. We additionally present an experimental validation of COFFEE for low orders aberrations using an in-house Adaptive Optics Bench and an apodized Roddier & Roddier phase mask coronagraph.

Keywords: wave-front sensing, high angular resolution, high contrast imaging, phase diversity, exoplanet detection

1. INTRODUCTION

Exoplanet detection is one of the main challenges of today's astronomy. A direct observation of these planets would provide information on the chemical composition of their atmospheres, or their temperatures. Such observations have recently been made possible,[1,2,3] but only thanks to their high mass or their wide apparent distance from their host star.
Being able to image an object as faint as an extra-solar planet very close to its parent star require the use of extreme AO (XAO) systems and a high-contrast imaging technique such as coronagraphy. Instruments dedicated to exoplanet imaging using these two techniques (SPHERE on the VLT , GPI on Gemini North) are being integrated. The performance of such systems is limited by residual speckles on the detector. These speckles originate in quasi-static Non Common Path Aberrations (NCPA), which strongly decrease the extinction provided by the coronagraph. In order to achieve the ultimate system performance, these aberrations must be measured and compensated for. Several techniques dedicated to high-contrast imaging system optimization have been proposed : SCC[4] , Speckle Nulling,[5] EFC,[6] CLOWFS.[7]
We have recently proposed a focal-plane wave-front sensor, COFFEE,[8] which is an extension of conventional phase diversity to a coronagraphic system. Since COFFEE uses focal-plane images, it is possible to characterize the whole bench without any differential aberration. Using these two images and an analytical model for coronagraphic imaging, we minimise a criterion in order to measure aberrations upstream and downstream of the coronagraph. COFFEE's principle and its application to the Apodized Roddier & Roddier Phase Mask (ARPM) are described in section 2. In section 3, we evaluate the quality of NCPA estimation by realistic simulations. In section 4, we present the experimental results from the laboratory demonstration of COFFEE on a in-house Adaptative Optics Bench (BOA) with an ARPM. Section 5 concludes the paper.

Further author information: (Send correspondence to B. Paul)
B. Paul: E-mail: baptiste.paul@onera.fr, Telephone: +33 (0)1 46 73 94 10

2. COFFEE : PRINCIPLE

2.1 Coronagraphic imaging model

Our wave-front sensor, COFFEE, uses the analytical coronagraphic imaging model developed by Sauvage & al.[9] Fig.1 describe the instrument principle.

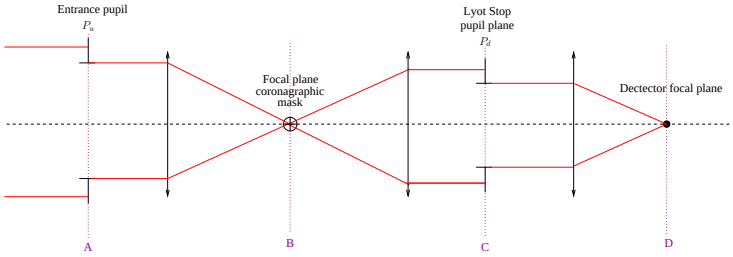

Figure 1. Coronagraphic imaging instrument : principle

Notations used in this paper will be those of Sauvage & al.[9] and Soummer & al.[10] We consider four successive planes denoted A (circular entrance pupil), B (coronagraphic focal plane), C (Lyot Stop) and D (detector plane). $\boldsymbol{r}$ is the pupil plane position vector, r its modulus and $\boldsymbol{\alpha}$ is the focal plane position vector. The entrance pupil function $P_u(\boldsymbol{r})$ is such as :

$$P_u(\boldsymbol{r}) = \Pi\left(\frac{r}{D_u}\right)\Phi(\boldsymbol{r}) \tag{2.1}$$

With $\Pi\left(\frac{r}{D_u}\right) = 1$ for $r \leq D_u$, pupil entrance diameter, and 0 otherwise. Φ is an apodization function. Considering only static aberrations (no residual turbulent aberrations), we distinguish aberrations introduced upstream of the coronagraph (NCPA), denoted $\phi_u(\boldsymbol{r})$ and assumed to be introduced in the entrance pupil plane A, and downstream of the coronagraph, denoted $\phi_d(\boldsymbol{r})$ and assumed to be introduced in the Lyot Stop pupil plane C. Thus, the electric field Ψ_A in the entrance pupil plane can be written as :

$$\Psi_A(\boldsymbol{r}) = P_u(\boldsymbol{r})e^{j\phi_u(\boldsymbol{r})} \tag{2.2}$$

The field amplitude $\Psi_B(\boldsymbol{\alpha})$ in plane B can be calculated, following Sauvage & al.,[9] using the analytical coronagraphic imaging model (which will be called "perfect coronagraph model" afterwards):

$$\Psi_B(\boldsymbol{\alpha}) = \mathrm{FT}^{-1}(\Psi_A(\boldsymbol{r})) - \eta_0\mathrm{FT}^{-1}(P_u(\boldsymbol{r})) \tag{2.3}$$

where η_0 is the value that minimise the outcoming energy from focal plane B, whose analytical value is given by :

$$\eta_0 = \frac{1}{\mathcal{N}}\iint_S \Psi_A^*(\boldsymbol{r})P_u(\boldsymbol{r})d\boldsymbol{r} \tag{2.4}$$

The normalisation factor $\mathcal{N}$ is defined such as $\eta_0 = 1$ when there is no aberration upstream of the coronagraph ($\phi_u(\boldsymbol{r}) = 0$), in order to have $\Psi_B = 0$ in such case (no aberrations in entrance pupil leads to no outcoming energy from plane B, and thus to a perfect extinction in the detector plane D):

$$\mathcal{N} = \iint_S |P_u|^2(\boldsymbol{r})d\boldsymbol{r} \tag{2.5}$$

Propagating the wave from plane B (Eq. 2.3) to plane D, we can write the electric field $\Psi_D(\boldsymbol{\alpha})$ in the detector plane :

$$\Psi_D(\boldsymbol{\alpha}) = \mathrm{FT}^{-1}(P_d(\boldsymbol{r})e^{j(\phi_u(\boldsymbol{r})+\phi_d(\boldsymbol{r}))}) - \eta_0\mathrm{FT}^{-1}(P_d(\boldsymbol{r})e^{j\phi_d(\boldsymbol{r})}) \tag{2.6}$$

$P_d(\boldsymbol{r})$ is the Lyot Stop pupil function: $P_d(\boldsymbol{r}) = \Pi\left(\frac{r}{D_d}\right)P_u(\boldsymbol{r})$ with D_d the Lyot Stop pupil diameter ($D_d \leq D_u$). For the sake of simplicity, we shall omit the spatial variables $\boldsymbol{r}$ and $\boldsymbol{\alpha}$ in the following. The coronagraphic "Point Spread Function" (PSF) of the instrument, denoted $\boldsymbol{h}_c$ is the square modulus of Ψ_D :

$$\boldsymbol{h}_c(\phi_u, \phi_d) = |\mathrm{FT}^{-1}(P_d e^{j(\phi_u+\phi_d)}) - \eta_0\mathrm{FT}^{-1}(P_d e^{j\phi_d})|^2 \tag{2.7}$$

2.2 COFFEE : coronagraphic phase diversity

COFFEE, which consist mainly in an extension of classical phase diversity to a coronagraphic imaging system, uses two images $\boldsymbol{i}_c^{\mathrm{f}}$ and $\boldsymbol{i}_c^{\mathrm{d}}$ that differ from a known aberration ϕ_{div} to estimate both phases upstream (ϕ_u) and downstream (ϕ_d) the coronagraph. We use here the imaging model presented in,[8] improved with a background term :

$$\begin{aligned}\boldsymbol{i}_c^{\mathrm{f}} &= f.\boldsymbol{h}_{\mathrm{d}} \star \boldsymbol{h}_c(\phi_u, \phi_d) + \boldsymbol{n} + b \\ \boldsymbol{i}_c^{\mathrm{d}} &= f.\boldsymbol{h}_{\mathrm{d}} \star \boldsymbol{h}_c(\phi_u + \phi_{div}, \phi_d) + \boldsymbol{n'} + b\end{aligned} \tag{2.8}$$

where f is the recorded flux, $\boldsymbol{h}_{\mathrm{d}}$ the known detector PSF, $\boldsymbol{n}$ and $\boldsymbol{n'}$ are the measurement noises, b is a uniform background (offset). $\star$ denote the discrete convolution operation.

The measurement noises $\boldsymbol{n}$ and $\boldsymbol{n'}$ comprise both photon and detector noises. Because calibration is assumed to be performed with high photon levels, we adopt a non-stationary white Gaussian model, which is a good approximation of a mix of photon and detector noises. Its variance is the sum of the photon and detector noise variances: $\sigma_n^2(k,l) = \sigma_{\mathrm{ph}}^2(k,l) + \sigma_{\mathrm{det}}^2$. The former can be estimated as the image itself thresholded to positive values, and the latter can be calibrated prior to the observations.

We adopt a Maximum *a posteriori* MAP approach and estimate the aberrations, the flux f and the background b that are most likely given our recorded images and our prior information on the aberrations. This approach aims to minimise the neg-log-likelihood of the data, potentially penalized by regularization terms on ϕ_u and ϕ_d designed to enforce smoothness of the sought phases:

$$(\hat{f}, \hat{b}, \hat{\phi_u}, \hat{\phi_d}) = \underset{f,b,\phi_u,\phi_d}{\operatorname{argmin}} J(f, b, \phi_u, \phi_d) \tag{2.9}$$

where

$$\begin{aligned}J(f, b, \phi_u, \phi_d) =& \frac{1}{2}\left\| \frac{\boldsymbol{i}_c^{\mathrm{f}} - (f.\boldsymbol{h}_{\mathrm{d}} \star \boldsymbol{h}_c(\phi_u, \phi_d) + b)}{\sigma_n} \right\|^2 \\ &+ \frac{1}{2}\left\| \frac{\boldsymbol{i}_c^{\mathrm{d}} - (f.\boldsymbol{h}_{\mathrm{d}} \star \boldsymbol{h}_c(\phi_u + \phi_{div}, \phi_d) + b)}{\sigma'_n} \right\|^2 \\ &+ \mathcal{R}(\phi_u) + \mathcal{R}(\phi_d)\end{aligned} \tag{2.10}$$

where $\|\boldsymbol{x}\|^2$ denotes the sum of squared pixel values of map $\boldsymbol{x}$, σ_n and $\sigma_{n'}$ are the noise variance maps of each image, and $\mathcal{R}$ is a regularization metric for the phase.
Any aberration ϕ is expanded on a basis b_k, which is typically either Zernike polynomials or the pixel indicator functions in the corresponding pupil plane : $\phi = \sum_k \phi_k b_k$ where the summation is, in practice, limited to the number of coefficients considered sufficient to correctly describe the aberrations. In this communication, the phase will be expanded on a truncated Zernike basis, which ensure the smoothness of the phase. Thus, no regularization metric is needed. Here, we will consider an aberration $\phi = \sum_k a_k Z_k$, with a_k the set of Zernike aberrations coefficients and Z_k the Zernike polynomial basis.
The minimization of metric $J(f, b, \phi_u, \phi_d)$ of Eq. (2.10) is performed by means of a Levenberg-Marquardt algorithm, which is a fast quasi-Newton type minimization method. It uses both gradients $\frac{\partial J}{\partial \phi_u}$ and $\frac{\partial J}{\partial \phi_d}$. Flux f and background b are analytically obtained as well using gradients $\frac{\partial J}{\partial f}$ and $\frac{\partial J}{\partial b}$ (implementation details, including gradient expressions, can be found in Appendix A).

In a previous communication,[8] it has been established that a suitable diversity phase ϕ_{div} for COFFEE was a mix composed of defocus and astigmatism : $\phi_{div} = a_4^{div} Z_4 + a_5^{div} Z_5$ with $a_4^{div} = a_5^{div} = 0.8$ rad RMS. We therefor use thise diversity phase in the following.

3. PERFORMANCE ASSESSMENT BY SIMULATION

The Roddier & Roddier Phase Mask (RRPM)[11,12] consist in a π phase shifting mask slightly smaller than the Airy disk. The use of a circular prolate function as entrance pupil apodization Φ, proposed by Soummer & al.[10] leads in a perfect case (no aberrations upstream the coronagraph) to a total suppression of signal in the detector plane. We have already demonstrated that ARPM images are compatible with the perfect coronagraph model and therefore with COFFEE estimation.[8] Realistic ARPM coronagraphic images are computed following Soummer & al.'s work[13] to avoid focal plane phase mask sampling

problems. Then, we use COFFEE to reconstruct both phases upstream and downstream the coronagraph. Notice that here, using the formalism developed in section 2.1, the prolate apodization function Φ is included in both simulation and reconstruction imaging models. In order to evaluate COFFEE's performance, we define a reconstruction error ϵ_x (x stands for u (upstream) or d (downstream)) per Zernike mode as :

$$\epsilon = \sqrt{\frac{1}{N}\sum_{k=0}^{N-1} |a_k - \hat{a}_k|^2} \tag{3.1}$$

With a_k the Zernike coefficients used for the simulation, $\hat{a}_k$ the reconstructed Zernike coefficients and N the number of reconstructed Zernike modes. In this section, we present the evolution of this reconstruction error with respect to the incoming flux, to an error made on the assumed diversity phase used in the reconstruction, and to the number of Zernike modes used in the reconstruction.

3.1 SNR : noise propagation

The ultimate limitation of an instrument lies in the quantity of noise in the images. In Figure 2, we present the reconstruction error for the aberrations upstream (ϕ_u) and downstream (ϕ_d) of the coronagraph with respect to the total incoming flux for two different types of simulations : one with the perfect coronagraph model, another with an ARPM; in both cases, reconstruction is performed assuming a perfect coronagraph. Simulation parameters are gathered in Table 1

Simulation	
images size	128×128 pixels
Sampling	2 pixels (Shannon)
ϕ_u : WFE	0.33 rad RMS
ϕ_d : WFE	0.13 rad RMS
Zernike basis used for ϕ_u and ϕ_d simulation	36 Zernike polynomials
noise	photon noise, detector noise ($\sigma_{\text{det}} = 5$ e$^-$)
Phase retrieval : COFFEE	
Zernike basis used for ϕ_u and ϕ_d reconstruction	36 Zernike polynomials

Table 1. COFFEE: simulation parameters for the noise propagation study

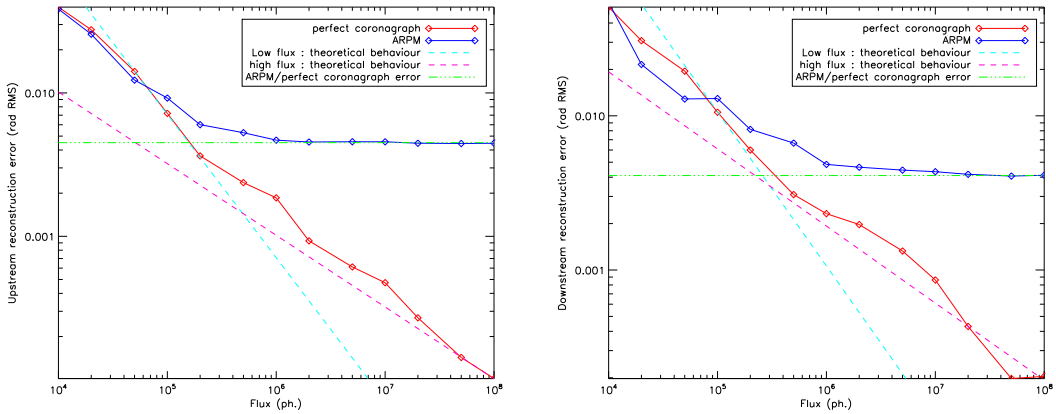

Figure 2. Aberrations upstream (ϕ_u, left) and downstream ((ϕ_d, right) the coronagraph : reconstruction error as a function of the incoming flux. For comparison, $\frac{1}{f}$ (cyan dashed line) and $\frac{1}{\sqrt{f}}$ (magenta dashed line) theoretical behaviours are plotted. Solid red line : image simulation with the perfect coronagraph model. Solid blue line : image simulation with an ARPM

For simulated images using the perfect coronagraph model (solid red line on figure 2), the evolution of the reconstruction error shows the two expected behaviours at low flux (detector noise limited ($\frac{1}{f}$)) and high flux (photon noise

limited ($\frac{1}{\sqrt{f}}$)). The perfect coronagraph model response to aberrations is very close to the one of the ARPM, which is why COFFEE is able to perform phase reconstructions using ARPM simulated images. However, because the image formation model used for simulation (ARPM) is not identical to the one used by COFFEE (perfect coronagraph), we have a threshold error (let us call it model error), which is the ultimate limit we can reach using the perfect coronagraph model. This model error can be clearly seen on Figure 2 : in the ARPM simulated images (solid blue line) case, both reconstruction errors reach a saturation level (green doted-dashed lines) which is $\epsilon_u^{\text{model}} = 4.5\ 10^{-3}$ rad RMS per mode (8% WFE) for ϕ_u.

3.2 Sensitivity to a diversity phase error

The diversity phase $\phi_{div} = a_4^{div} Z_4 + a_5^{div} Z_5$ has been defined in section 2.2 as a mix of defocus and astigmatism. This phase ϕ_{div} is one of the input COFFEE needs in order to perform phase retrieval, and thus requires to be calibrated. In order to optimize the use of COFFEE, the impact of an error on such a calibration must be studied. In this section, we will consider that the phase diversity used to create the diversity image is not perfectly known : coronagraphic simulated diversity image will be computed with a diversity phase $\hat{\phi}_{div} = \phi_{div} + \phi_{err}$, with ϕ_{err} a randomly generated phase of given WFE. COFFEE's phase reconstruction will be done considering that the diversity phase is equal to ϕ_{div}. Others parameters of this simulation are gathered in Table 2

Simulation	
images size	128×128 pixels
Sampling	Shannon
ϕ_u : WFE	0.33 rad RMS
ϕ_d : WFE	0.13 rad RMS
Error on diversity ϕ_{err} : WFE	from 0 to 0.1 rad RMS
Zernike basis used for ϕ_u and ϕ_d simulation	36 Zernike polynomials
noise	none
COFFEE : phase retrieval	
Zernike basis used for ϕ_u and ϕ_d reconstruction	36 Zernike polynomials

Table 2. COFFEE: simulation parameters for the study of the error on diversity phase

In order to consider only the impact of an error on the diversity phase, coronagraphic simulated images are computed using the perfect coronagraph, and not an ARPM model (thus, there is no model error in this simulation). In a realistic case, we assume to have a good knowledge of the introduced diversity phase. Thus, we only consider here small WFE (with respect to ϕ_{div}) for the error ϕ_{err}.

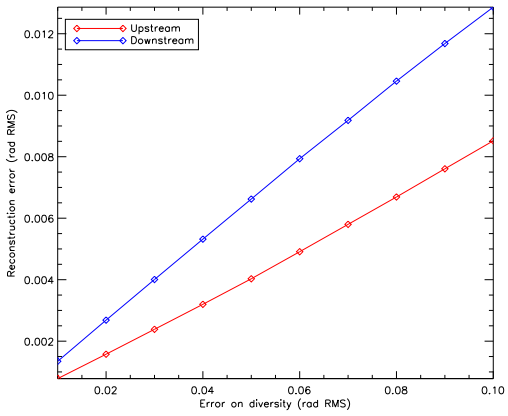

Figure 3. Error reconstructions upstream (solid red line) and downstream (solid blue line) the coronagraph as functions of the error on the diversity phase.

As expected, both reconstruction errors increase with the error on diversity ϕ_{err} WFE. In section 3.1, we showed that the ultimate limit of COFFEE lies in the use of the perfect coronagraph model. Thus, a calibration of the diversity phase

which gives us a reconstruction error of the same level of the model error $\epsilon_u^{\text{model}}$ will be accurate enough. Simulations show that for any WFE, the model error is 8% of this WFE, which gives us the required accuracy level of calibration for ϕ_{div}.

3.3 Impact of aliasing on reconstruction error

Since the phase estimation is performed on a truncated Zernike basis, we have to determine the size of such a basis, i.e. the number of Zernike modes to be used for the phase reconstruction. On our bench, we are able to compensate for the first 15 Zernike modes. The estimation accuracy on these 15 modes will be limited by an aliasing error, which originate in the impact of high order aberrations (not expandable on the truncated basis) on the estimated Zernike mode. In order to reduce the error on these 15 modes, it is necessary to estimate at least twice more Zernike modes. Thus, we chose to estimate 36 Zernike modes to reconstruct both phases upstream (ϕ_u) and downstream (ϕ_d) the coronagraph.
The impact of the aliasing on the phase reconstruction have been quantified by a realistic simulation, which aim is to gives us the aliasing error value for our in-house bench: we measured the aberrating wavefront on our bench using a commercial Hartmann-Shack wave-front sensor sold by Imagine Optic; then, we added to this measured wavefront a random aberration expanded on the first 15 Zernike modes. Using this wave-front, we compute coronagraphic images using the perfect coronagraph model (no model error). Then, we perform phases reconstruction on 36 Zernike modes with COFFEE. This simulation gives us the aliasing error $\epsilon_{\text{aliasing}}$ (calculated using Eq. 3.1): for the first 15 reconstructed Zernike modes, $\epsilon_{\text{aliasing}_{15}} = 1.4\ 10^{-2}$ rad RMS per modes ; for the 36 reconstructed modes, $\epsilon_{\text{aliasing}_{36}} = 2.7\ 10^{-2}$ rad RMS per modes.

4. LABORATORY DEMONSTRATION

In this section we present experimental validations of the coronagraphic phase diversity. These validations have been done on the ONERA Adaptive Optics bench BOA, described in section 4.1. . Section 4.2 describe an experimental way of introducing calibrated static aberrations on the AO bench to be measured with COFFEE. In section 4.3, we explains the static aberrations measurement, while section 4.4 details the compensation process.

4.1 Experimental setup

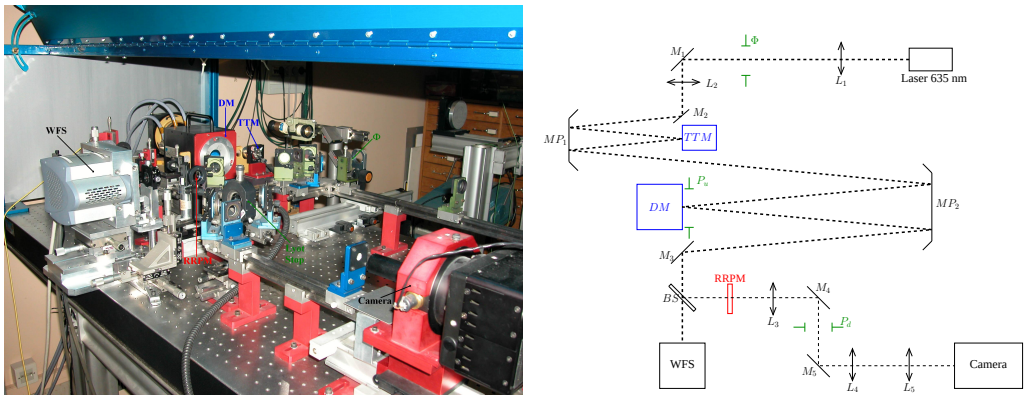

Figure 4. Experimental Setup. Left : bench BOA. Right : schematic representation. M_i : plane mirrors ; MP_i : parabolic mirrors ; L_i : lenses (doublets); BS : beam splitter ; TTM : Tip-Tilt mirror ; DM : Deformable mirror ; $RRPM$: coronagraphic phase mask ; Φ : prolate apodizer ; WFS : AO wave-front sensor

Figure 4 shows the design of our in-house bench. The input beam, emitted from a fibred laser source ($\lambda = 635$ nm) comes through the prolate apodizer Φ, which is in a pupil plane conjugated with the entrance pupil plane (P_u). The beam is reflected by the Tip-Tilt mirror (TTM) and then on the deformable mirror (DM, entrance pupil, $D_u = 40$ mm, 6×6 actuators). The beam-splitter BS send a fraction of the beam to the AO wave-front sensor (Shack-Hartmann, 5×5 sub-pupil matrix). On the other channel, the light is focused onto a Roddier & Roddier Phase Mask (RRPM), whose diameter is $d_{RRPM} = 18.1$ μm (angular diameter is $1.06\frac{\lambda}{D_u}$). After coming trough the Lyot Stop plane (P_d, with $D_d = 0.99D_u$), the beam is focused onto the camera (256×256 pixels images with an oversampling of a factor 2.75, detector noise $\sigma_{\text{det}} = 1$ e$^-$). For faster computations, recorded images are re-sized to 128×128 pixels images with an oversampling of a factor 1.375.

4.2 Introduction of calibrated aberrations

In order to evaluate COFFEE's estimation performances, we have introduced on the bench calibrated aberrations using a process described in this section. Let us consider an aberrating phase ϕ_{cal} we want to introduce on BOA. Because the DM introduce a phase using a finit number of actuators (6×6), the introduced aberration will not match perfectly the aberration ϕ_{cal}, as illustrated on figure 5 in the case of a pure spherical aberration.

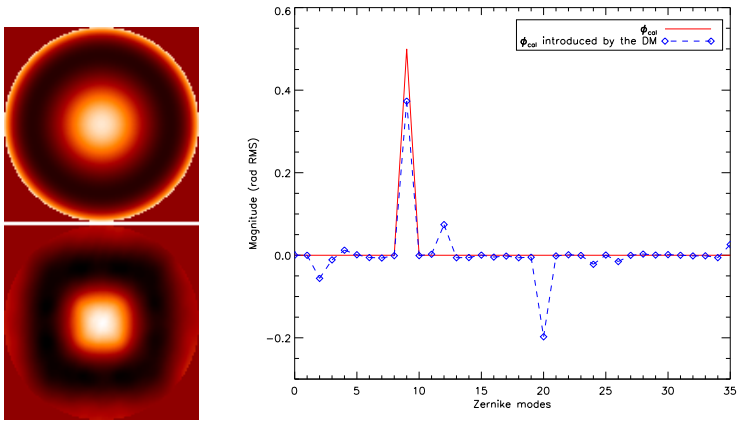

Figure 5. Introduction of calibrated aberration on BOA : case of a pure spherical aberration. Left : theoretical wave-front (top) and DM introduced wave-front (bottom). Right : corresponding Zernike modes for the theoretical introduced aberration (solid red line) and the DM introduced aberration (dashed blue line).

Our aim is here to introduce, using the DM, the closest aberration to the aberration ϕ_{cal}. Let F be the DM influence matrix; any DM introduced aberration ϕ^{DM} can be described as a set of actuator voltages u ($\phi^{DM} = Fu$). We are thus looking for the set u_{cal} which solve the least-square problem:

$$u_{cal} = \underset{u}{\text{argmin}} \, \|Fu - \phi_{cal}\|^2 \tag{4.1}$$

The solution of this problem can be written as:

$$u_{cal} = T\phi_{cal} \tag{4.2}$$

With T the generalized inverse of matrix F. Using the interaction matrix D, we can calculate the corresponding set of slopes s_{cal} ($s_{cal} = Du_{cal}$). This set of slopes can then be used to modify the AO loop reference slopes s_{ref}. Thus, closing the AO loop with the slopes $s_{\text{ref}} + s_{cal}$, we introduce on the bench an aberration ϕ_{cal}^{DM}, which is the best fit of ϕ_{cal} in the least square sense.
We have also to consider that the bench BOA presents its own unknown static aberrations ϕ_u^{BOA} and ϕ_d^{BOA} upstream and downstream of the coronagraph (respectively). Thus, if a calibrated aberrations ϕ_{cal} is introduced in the entrance pupil, aberrations ϕ_u upstream of the coronagraph will be :

$$\phi_u = \phi_{cal} + \phi_u^{\text{BOA}} \tag{4.3}$$

In order to get rid of the unknown aberration ϕ_u^{BOA}, we perform a differential phase estimation :

1. We introduce the aberration ϕ_{cal} on the bench. A phase $\hat{\phi}_u^+ = \hat{\phi}_{cal} + \hat{\phi}_u^{BOA}$ is estimated using focused and diversified images recorded on the camera.
2. the opposite aberration $-\phi_{cal}$ is then introduced. A phase $\hat{\phi}_u^- = -\hat{\phi}_{cal} + \hat{\phi}_u^{BOA}$ is estimated.
3. The half-difference $\hat{\phi}_{cal} = \frac{\hat{\phi}_u^+ - \hat{\phi}_u^-}{2}$ is our estimate of ϕ_{cal}

4.3 NCPA measurements

In order to take into account the DM action on the introduced phase, aberration ϕ_{cal} are first estimated with classical phase diversity (no phase mask in the coronagraphic focal plane).[14] This estimation gives us an accurate calibration of the introduced aberration, which is then used to evaluate the accuracy of COFFEE's introduced aberration estimation.

We give here the error budget for COFFEE's aberrations estimation upstream of the coronagraph on BOA for an introduced phase ϕ_{cal} (WFE $= 80$ nm (0.80 rad RMS at $\lambda = 635$ nm) expanded on the first 15 Zernike modes:

- ◇ Photon and detector noises error : $\epsilon_{\text{noise}} = 1.6\ 10^{-3}$ rad RMS per mode. This value has been calculated from simulation presented in section 3.1.
- ◇ From simulations, we know that the model error is 8% of WFE. Knowing this, we calculate $\epsilon_{\text{model}} = 1.1\ 10^{-2}$ rad RMS per mode for WFE$= 0.8$ rad RMS.
- ◇ The diversity phase ϕ_{div} has been calibrated using classic phase diversity. Such an estimation have been performed with an error of $6.7\ 10^{-3}$ rad RMS. According to section 3.2, such an error on the diversity phase leads to an error $\epsilon_{\text{model}} = 5.0\ 10^{-3}$ rad RMS per mode.
- ◇ The presence of a resolved object, not included in our image formation model, will have an impact on phase estimation. Since the coronagraph presence implies a non convolutive imaging model, it is complicated to accurately quantifiy the error due to this parameter. The value we calculated comes from a crude simulation, where we consider the imaging system as convolutive: $\epsilon_{\text{obj}} = 1.4\ 10^{-2}$ rad RMS per mode.
- ◇ Residual turbulent speckles, which originate in uncorrected turbulent aberrations, are not included in the imaging model. In order to measure the impact of these speckle on the reconstruction, a large number of wave-fronts have been successively recorded. From these aquisitions, we calculate a residual turbulent wave-front error $\epsilon_{\text{turb}} = 2.0\ 10^{-3}$ rad RMS per mode.
- ◇ Aliasing error, which originate in high order aberration, has been given in section 3.3 : $\epsilon_{\text{aliasing}_{36}} = 2.7\ 10^{-2}$ rad RMS per mode

Table 3 gathers the error budget values.

Noise	$\epsilon_{\text{noise}} = 1.6\ 10^{-3}$ rad RMS per mode
Model error	$\epsilon_{\text{model}} = 1.0\ 10^{-2}$ rad RMS per mode
Error on diversity	$\epsilon_{\text{div}} = 5.0\ 10^{-3}$ rad RMS per mode
Resolved object	$\epsilon_{\text{obj}} = 1.4\ 10^{-2}$ rad RMS per mode
Residual turbulence	$\epsilon_{\text{turb}} = 2.0\ 10^{-3}$ rad RMS per mode
Aliasing	$\epsilon_{\text{aliasing}_{36}} = 2.7\ 10^{-2}$ rad RMS per mode
Total error	$\epsilon = \sqrt{\sum_i \epsilon_i^2} = 3.3\ 10^{-2}$ rad RMS per mode

Table 3. COFFEE : error budget for the estimation of an aberration expanded on the first 15 Zernike modes introduced on BOA.

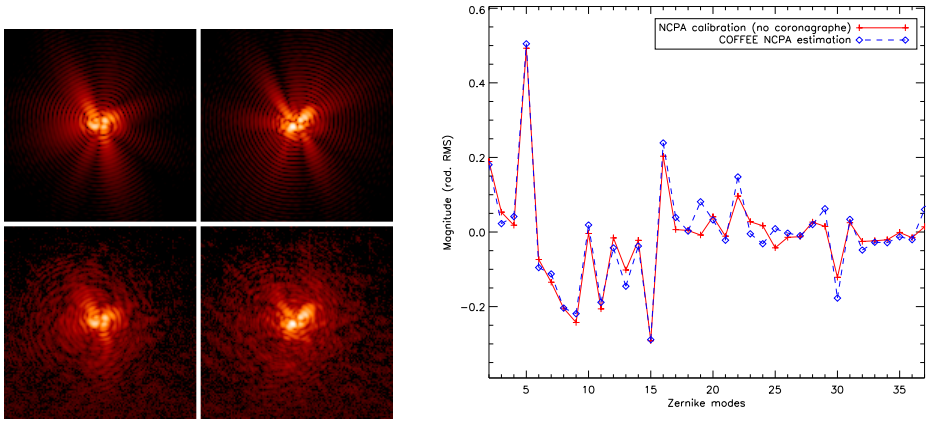

Figure 6. COFFEE : NCPA estimation. Estimation of a randomly introduced phase ϕ_{cal} on BOA. Right : Zernike modes calibrated using phase diversity (solid red line) and estimated by COFFEE (dashed blue line). Left : focused (left) and diversified (right) coronagraphic images for an introduced aberration ϕ_{cal}, recorded from the camera (bottom) and computed (top) with the reconstructed aberrations.

At the convergence of the reconstruction, a very good match can be observed between the experimental images and the ones computed for the estimated aberrations (figure 6, left). This results, in term, in a very good match between the Zernike modes measured by COFFEE and the introduced calibrated aberrations (figure 6, right).
According to the error budget, the assumed reconstruction error per mode for the 36 reconstruced modes is:

$$\epsilon_{\text{sim}_{36}} = \sqrt{\epsilon^2_{\text{aliasing}_{36}} + \epsilon^2_{\text{turb}} + \epsilon^2_{\text{noise}} + \epsilon^2_{\text{obj}} + \epsilon^2_{\text{div}} + \epsilon^2_{\text{model}}} = 3.3\ 10^{-2} \text{ rad RMS per mode} \tag{4.4}$$

From the experimental phase estimation presented in figure 6, we calculate a reconstruction error:

$$\epsilon_{\text{exp}_{36}} = 3.1\ 10^{-2} \text{ rad RMS per mode} \tag{4.5}$$

In section 3.3, we gave the aliasing error for the first 15 Zernike mode: $\epsilon_{\text{sim}_{15}} = 1.4\ 10^{-2}$ rad RMS per mode. Considering that the aliasing error is the main contribution to the error budget, we assume that the others terms doesn't change with the size of the considered truncated Zernike basis. Thus, for the first 15 Zernike modes, we calculate:

$$\epsilon_{\text{sim}_{15}} = \sqrt{\epsilon^2_{\text{aliasing}_{15}} + \epsilon^2_{\text{turb}} + \epsilon^2_{\text{noise}} + \epsilon^2_{\text{obj}} + \epsilon^2_{\text{div}} + \epsilon^2_{\text{model}}} = 2.3\ 10^{-2} \text{ rad RMS per mode} \tag{4.6}$$

Experimental phase estimation presented in figure 6 gives us:

$$\epsilon_{\text{exp}_{15}} = 2.3\ 10^{-2} \text{ rad RMS per mode} \tag{4.7}$$

In both case (for 15 or 36 Zernike modes), our error budget gives us an accurate value of the global reconstruction error. Knowing this, we will be able to use this budget to know the limitations of COFFEE and think of a way to minimize their impact.

4.4 NCPA measurements and compensation

Lastly, the ability of COFFEE to compensate for the aberrations upstream of the coronagraph is experimented on BOA. As we said previously, with our 6x6 DM, correction is limited to the first 15 Zernike modes. In order to demonstrate the ability of COFFEE to be used in a closed loop, we introduce a set of aberrations on the DM by modifying the reference slopes, as described in section 4.2. Then, we use the pseudo-closed loop (PCL) method described in.[14] This iterative process has two stages: for the PCL iteration i:

1. Estimation of the aberration $\hat{\phi}^i_u$ upstream the coronagraph
2. Correction of the current NCPA ϕ_i considering that $\phi^i = \phi^{i-1} - g_{\text{PCL}}\hat{\phi}^i_u$, where g_{PCL} is the PCL gain.

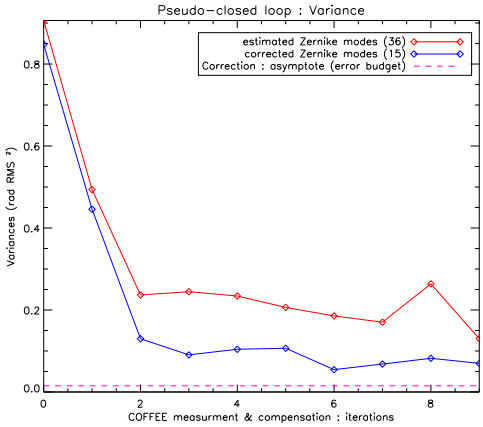

Figure 7. PCL on the bench BOA ($g_{\mathrm{PCL}} = 0.5$) : variance of the residual static aberrations upstream the coronagraph for the 36 COFFEE estimated Zernike modes (solid red line) and the 15 corrected modes (solid blue line). The magenta dashed line represent the ultimate performance we can reach according to the error budget established in section 4.3

The correction and stabilisation of the NCPA variance can be seen on figure 7. One can note that the performance assumed according to the error budget is not exactly reached. This is partly due to the performances of the AO system of BOA. Indeed, with our 6×6 actuators DM, Zernike modes are not perfectly introduced on the bench : this phenomenon has been showed on figure 5, where we showed that a spherical aberration cannot be introduced without several others Zernike modes. Thus, in the PCL process, when a phase is introduced on the bench, we introduce some extra-aberrations as well which originates in this phenomenon. We are currently working on the precise quatification of this error term. A demonstration of COFFEE's abilities to significantly compensate for the aberrations upstream of the coronagraph would involve a deformable mirror with a larger number of actuators (for a better compensation) and an improved estimation method which would leads to a lower error budget. Still, with this first pseudo-closed loop, we show that COFFEE can be used in an iterative process to minimize the variance of the phase upstream of the coronagraph.

5. CONCLUSION

In this communication, we have presented a first experimental validation of our coronagraphic wave-front sensor called COFFEE, which consists mainly in the extension of the phase diversity concept to a coronagraphic imaging system. From the validation and performance assessment of COFFEE presented in section 3, we demonstrated that the two factors that limit COFFEE's phase estimation accuracy are currently the model error, which originate in the use of a coronagraphic analytical model (evaluated in section 2), and the aliasing error, due to high order aberrations, which are difficult to model with a Zernike basis. From these simulations, we have evaluate the expected error on COFFEE's phase estimation for our in-house bench, which is $\epsilon = 3.3$ nm RMS per mode on 36 Zernike modes.
In section 4, we have presented a first experimental validation of COFFEE using an apodized Roddier & Roddier phase mask. We have introduced calibrated aberrations upstream of the coronagraph (NCPA), using the AO sub-system, and estimated them with COFFEE. The accuracy we obtained on these estimation shows a very good match with our error budget. Lastly, we used COFFEE in an iterative process to compensate for aberrations upstream the coronagraph.
Several perspectives are currently considered to optimize COFFEE : as we said previously, the error model is one limiting factor of our phase estimation. One of the improvements of our wave-front sensor will thus consist in the development of a more accurate imaging model. Such a model, which could include a residual turbulent aberration, will ultimately allow us to perform NCPA estimation on images from the sky. Alternatively, a simple model for the case where there is no residual turbulence is obtained by propagating the electric field through each plane of the coronagraphic imaging system (figure 1) for an arbitrary focal plane coronagraphic mask; such a method, where no model error needs to be considered, can be used for a laboratory calibration.
Besides, in order to minimize the impact of the aliasing error on the phase reconstruction, we are implementing the phase reconstruction on a pixel-wise map, more suitable than a truncated Zernike basis.

Acknowledgments

The authors thank the Région Provence-Alpes-Côte d'Azur for partial financial support of B. Paul's scholarship.

APPENDIX A. IMPLEMENTATION DETAILS

COFFEE performs a phase estimation minimizing the criterion whose expression is given by equation 2.10. Since the estimation is done on a truncated Zernike base, there is no need for regularization terms. Therefore, the criterion expression is :

$$J(f,b,\phi_u,\phi_d) = J^{\mathrm{f}}(f,b,\phi_u,\phi_d) + J^{\mathrm{d}}(f,b,\phi_u,\phi_d) \tag{A.1}$$

With :

$$\begin{aligned} J^{\mathrm{f}}(f,b,\phi_u,\phi_d) &= \frac{1}{2}\left\| \frac{\boldsymbol{i}_c^{\mathrm{f}} - (f.\boldsymbol{h}_d \star \boldsymbol{h}_c(\phi_u,\phi_d)+b)}{\sigma_n} \right\|^2 \\ J^{\mathrm{d}}(f,b,\phi_u,\phi_d) &= \frac{1}{2}\left\| \frac{\boldsymbol{i}_c^{\mathrm{d}} - (f.\boldsymbol{h}_d \star \boldsymbol{h}_c(\phi_u+\phi_{div},\phi_d)+b)}{\sigma'_n} \right\|^2 \end{aligned} \tag{A.2}$$

In order to estimate ϕ_u and ϕ_d, we need both gradients $\frac{\partial J}{\partial \phi_u}$ and $\frac{\partial J}{\partial \phi_d}$: Considering the expression of J, we will derive here J^{f} only. Then, a trivial substitution gives the gradients expressions of J^{d}. Let us write the numerical expression of J^{f} :

$$J^{\mathrm{f}}(f,b) = \frac{1}{2}\sum_{\boldsymbol{n}} \left| \frac{\boldsymbol{i}_c^{\mathrm{f}}[\boldsymbol{n}] - f.\boldsymbol{h}_d[\boldsymbol{n}] \star \boldsymbol{h}_c[\boldsymbol{n}] - b}{\sigma_n[\boldsymbol{n}]} \right|^2 \tag{A.3}$$

With $\boldsymbol{n}$ the pixel position in the detector plane.σ_n is the noise variance maps. The calculation will be done following Mugnier & al.:[15] first, we calculate the gradient of J^{f} with respect to the PSF $\boldsymbol{h}_c$:

$$\frac{\partial J^{\mathrm{f}}}{\partial \boldsymbol{h}_c} = \frac{1}{\sigma_n^2}[f\boldsymbol{h}_d(f.\boldsymbol{h}_d \star \boldsymbol{h}_c - \boldsymbol{i}_c^{\mathrm{f}})] \tag{A.4}$$

Then, calculation consist in calculating the gradient of the PSF $\boldsymbol{h}_c$ with respect to phases $\phi_u[\boldsymbol{k}]$ and $\phi_d[\boldsymbol{l}]$ at pixels $\boldsymbol{k}$, $\boldsymbol{l}$ in pupils upstream and downstream of the coronagraph (respectively) and applying the chain rule, as it has already been done in a non coronagraphic case in ref.[16]

$$\begin{aligned} \frac{\partial J^{\mathrm{f}}}{\partial \phi_u[\boldsymbol{k}]} &= 2(\Im(\psi^*[\boldsymbol{k}](\mathrm{TF}\left(\frac{\partial J^{\mathrm{f}}}{\partial\, \boldsymbol{h}_c}(\Psi - \eta_0\Psi_d)\right))[\boldsymbol{k}] - \Re\left(\frac{\partial \eta_0}{\partial \phi_u[\boldsymbol{k}]}\sum_{\boldsymbol{n}}\frac{\partial J^{\mathrm{f}}}{\partial\, \boldsymbol{h}_c}\Psi^*\Psi_d\right) + \frac{1}{2}\frac{\partial |\eta_0|^2}{\partial \phi_u[\boldsymbol{k}]}\sum_{\boldsymbol{n}}\frac{\partial J^{\mathrm{f}}}{\partial\, \boldsymbol{h}_c}|\Psi_d|^2) \\ \frac{\partial J^{\mathrm{f}}}{\partial \phi_d[\boldsymbol{l}]} &= 2\Im((\psi^*[\boldsymbol{l}] - \eta_0^*\psi_d^*[\boldsymbol{l}])(\mathrm{TF}\left(\frac{\partial J^{\mathrm{f}}}{\partial\, \boldsymbol{h}_c}(\Psi - \eta_0\Psi_d)\right))[\boldsymbol{l}]) \end{aligned} \tag{A.5}$$

With $\Im$ and $\Re$ the imaginary and real part (respectively), and :

$$\begin{aligned} \frac{\partial \eta_0}{\partial \phi_u} &= jP_u^2 e^{j\phi_u} \\ \psi(\phi_u,\phi_d) &= P_d e^{j(\phi_u+\phi_d)} \qquad \Psi(\phi_u,\phi_d) = \mathrm{TF}^{-1}(\psi) \\ \psi_d(\phi_d) &= P_d e^{j\phi_d} \qquad \Psi_d(\phi_d) = \mathrm{TF}^{-1}(\psi_d) \end{aligned} \tag{A.6}$$

Since we are expanding the phases on a Zernike basis, we need the gradients of J^{f} with respect to the Zernike modes a_i of phase ϕ_u. These gradients are given by the expression:[15]

$$\frac{\partial J^{\mathrm{f}}}{\partial a_i} = \sum_{\boldsymbol{k}} \frac{\partial J^{\mathrm{f}}}{\partial \phi_u[\boldsymbol{k}]} Z_i[\boldsymbol{k}] \tag{A.7}$$

Flux f and constant background b are also analytically estimated during the minimization. Considering that :

$$J^{\mathrm{f}}\boldsymbol{n} = \frac{1}{2}\sum_{\boldsymbol{n}} \left| \frac{-\boldsymbol{i}_c^{\mathrm{f}}[\boldsymbol{n}] + f.\boldsymbol{h}_d[\boldsymbol{n}] \star \boldsymbol{h}_c[\boldsymbol{n}] + b}{\sigma_n[\boldsymbol{n}]} \right|^2 \tag{A.8}$$

We have :

$$\begin{aligned} \frac{\partial J^{\mathrm{f}}}{\partial f} &= f\sum_{\boldsymbol{n}} \frac{(\boldsymbol{h}_d[\boldsymbol{n}] \star \boldsymbol{h}_c[\boldsymbol{n}])^2}{\sigma_n[\boldsymbol{n}]} + b\sum_{\boldsymbol{n}} \frac{\boldsymbol{h}_d[\boldsymbol{n}] \star \boldsymbol{h}_c[\boldsymbol{n}]}{\sigma_n[\boldsymbol{n}]} - \sum_{\boldsymbol{n}} \frac{(\boldsymbol{h}_d[\boldsymbol{n}] \star \boldsymbol{h}_c[\boldsymbol{n}])\boldsymbol{i}_c^{\mathrm{f}}[\boldsymbol{n}]}{\sigma_n[\boldsymbol{n}]} \\ \frac{\partial J^{\mathrm{f}}}{\partial b} &= f\sum_{\boldsymbol{n}} \frac{\boldsymbol{h}_d[\boldsymbol{n}] \star \boldsymbol{h}_c[\boldsymbol{n}]}{\sigma_n[\boldsymbol{n}]} + b\sum_{\boldsymbol{n}} \frac{1}{\sigma_n[\boldsymbol{n}]} - \sum_{\boldsymbol{n}} \frac{\boldsymbol{i}_c^{\mathrm{f}}[\boldsymbol{n}]}{\sigma_n[\boldsymbol{n}]} \end{aligned} \tag{A.9}$$

Which gives us, in a matricial form :

$$\begin{pmatrix} \sum_{\boldsymbol{n}} \frac{(\boldsymbol{h}_d[\boldsymbol{n}]\star\boldsymbol{h}_c[\boldsymbol{n}])^2}{\sigma_n[\boldsymbol{n}]} & \sum_{\boldsymbol{n}} \frac{\boldsymbol{h}_d[\boldsymbol{n}]\star\boldsymbol{h}_c[\boldsymbol{n}]}{\sigma_n[\boldsymbol{n}]} \\ \sum_{\boldsymbol{n}} \frac{\boldsymbol{h}_d[\boldsymbol{n}]\star\boldsymbol{h}_c[\boldsymbol{n}]}{\sigma_n[\boldsymbol{n}]} & \sum_{\boldsymbol{n}} \frac{1}{\sigma_n[\boldsymbol{n}]} \end{pmatrix} \begin{pmatrix} f \\ b \end{pmatrix} = \begin{pmatrix} \sum_{\boldsymbol{n}} \frac{(\boldsymbol{h}_d[\boldsymbol{n}]\star\boldsymbol{h}_c[\boldsymbol{n}])\boldsymbol{i}_c^{\mathrm{f}}[\boldsymbol{n}]}{\sigma_n[\boldsymbol{n}]} \\ \sum_{\boldsymbol{n}} \frac{\boldsymbol{i}_c^{\mathrm{f}}[\boldsymbol{n}]}{\sigma_n[\boldsymbol{n}]} \end{pmatrix} \tag{A.10}$$

A simple matrix inversion gives us the analytical estimation of the flux f and the background b for each iteration.

APPENDIX B. TIP-TILT ESTIMATION DOWNSTREAM OF THE CORONAGRAPH

We realised that the tip-tilt downstream the coronagraph (which represent the image position on the detector) could strongly limit COFFEE's performances. Indeed, we determine that the phase estimation was accurate when -1 rad RMS $\leq a_i \leq 1$ rad RMS, with a_i the Zernike coefficient for tip or tilt ($i \in \{2, 3\}$). Beyond this range, COFFEE is unable to properly estimate both phases ϕ_u and ϕ_d. Such a phenomenon strongly limits COFFEE's performance on a bench, since its utilisation requires a restrictive location of the PSF on the detector.

In order to get rid of this limitation, we have developed a simple and fast method in order to do an estimation of the tip-tilt downstream the coronagraph, based on the diversity image. This image is created by adding a known aberration $\phi_{div} = a_4^{div} Z_4 + a_5^{div} Z_5$ ($a_4^{div} = a_5^{div} = 0.8$ rad RMS) to ϕ_u. Since the amplitude of this aberration is important ($\sigma_{phi_{div}} = 113$ nm RMS at $\lambda = 635$ nm), the speckles we have in the coronagraphic diversity image should mainly originate in these diversity aberrations. This is illustrated on figure 8, where we show two diversity images : one computed with randomly generated phases ϕ_u (WFE 0.3 rad RMS)and ϕ_d (WFE 0.1 rad RMS), and another computed with no aberrations other than the diversity ones.

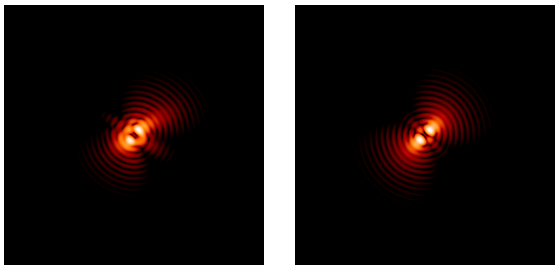

Figure 8. Coronagraphic diversity images computed for an aberration $\phi_u + \phi_{div}$ upstream, ϕ_d downstream (left) and the only diversity aberration ϕ_{div} (right).

As one can see on figure 8, we can clearly identify the aberrations which originate in the diversity ϕ_{div}. The principle of our method lies in the research of these well-known aberrations (since we know the phase ϕ_{div} we introduce) in the diversity image i_c^{d} by comparing it with a theoretical diversity image $i_{c_{th}}^{\mathrm{d}}$, calculated with no others aberrations than the diversity ones :

$$\boldsymbol{i}_{c_{th}}^{\mathrm{d}} = \boldsymbol{h}_d \star \boldsymbol{h}_c(\phi_{div}, \phi_d = 0) \tag{B.1}$$

The comparison of $i^{\mathrm{d}}_{c_{th}}$ with i^{d}_{c} is performed using the method developed by Gratadour & al.,[17] which consist in minimizing the following criterion J_{TT}

$$J_{\mathrm{TT}}(x,y) = \left\| \frac{i^{\mathrm{d}}_{c}(x_o,y_o) - i^{\mathrm{d}}_{c_{th}}(x_o,y_o) \star \delta(x_o - x, y_o - y)}{\sigma'_n} \right\|^2 \tag{B.2}$$

Minimization of J_{TT} gives us the shift $[x_M, y_M]$between both images. It is then possible to calculate the corresponding tip (a_2) and tilt (a_3) downstream the coronagraph knowing the image sampling s :

$$\begin{aligned} a_2 &= \frac{\pi}{2s} x_M \\ a_3 &= \frac{\pi}{2s} y_M \end{aligned} \tag{B.3}$$

Finally, these estimated tip-tilt values are given to COFFEE as an input of the minimization, and are used as initial values to begin phases reconstruction. Since images $i^{\mathrm{d}}_{c_{th}}$ and i^{d}_{c} are not the same, we will not have a very precise estimation. But we know that COFFEE is able to perform an accurate phase reconstruction if the tip-tilt downstream of teh coronagraph is known with a precision of $\pm$ 1 rad RMS. Thus, a rough estimation of tip-tilt is far enough to get rid of this limitation, as showed by the following simulation. Using the perfect coronagraph model (no reconstruction error), we computed focused and diversified coronagraphic images for randomly generated phases ϕ_u and ϕ_d. Besides, we add, in ϕ_d, a phase ϕ_d^{TT} expanded only on the tip-tilt Zernike modes, whose range is $[-5; 5]$ rad RMS. Then, COFFEE estimates $\hat{\phi}_u$ and $\hat{\phi}_d$ with and without a preliminary tip-tilt downstream the coronagraph estimation.

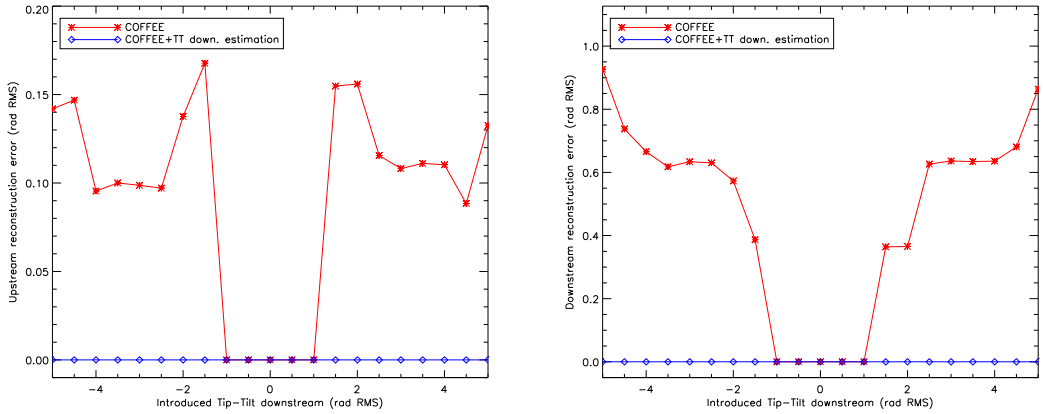

Figure 9. Error reconstruction upstream (left) and downstream (right) the coronagraph as a function of the Tip-Tilt downstream of the coronagraph a_2, a_3. Solid red line : reconstruction error with COFFEE. Solid blue line : reconstruction error with COFFEE and a preliminary tip-tilt downstream the coronagraph estimation

On figure 9, one can see that when the position of the PSF on the detector is unknown (no preliminary tip-tilt estimation), it is not possible to estimate a phase if the tip-tilt downstream of the coronagraph is beyond the range $[-1, 1]$ rad RMS. The use of our tip-tilt preliminary estimation method make the phase reconstruction accurate (reconstruction error upstream and downstream the coronagraph are 0 rad RMS per mode) for any tip-tilt value, and thus for any position of the coronagraphic image on the detector. This method uses only the diversity image and thus does not require any extra data acquisition, and perform and fast preliminar estimation (~ 1 second for a 256×256 image) of the tip-tilt downstream the coronagraph.

REFERENCES

[1] Kalas, P., Graham, J. R., Chiang, E., Fitzgerald, M. P., Clampin, M., Kite, E. S., Stapelfeldt, K., Marois, K., and Krist, J., "Optical images of an extrasolar planet 25 light years from earth," *Science* **332** (2008).

[2] Marois, C., Macintosh, B., Barman, T., Zuckerman, B., Song, I., Patience, J., Lafrenière, D., and Doyon, R., "Direct imaging of multiple planets orbiting the star hr 8799," *Science* **322** (2008).

[3] Lagrange, A.-M., Bonnefoy, M., Chauvin, G., Apai, D., Ehrenreich, D., Boccaleti, A., Gratadour, D., Rouan, D., Mouillet, D., Lacour, S., and Kasper, M., "A giant planet imaged in the disk of the young star beta pictoris," *Science* **329** (2010).

[4] Baudoz, P., Boccaletti, A., Baudrand, J., and Rouan, D., "The self-coherent camera : a new tool for exoplanet detection," in [*Proceeding IAU Colloquium*], (2006).

[5] Bordé, P. J. and Traub, W. A., "High constrast imaging from space : speckle-nulling in a low-aberration regime," *The Astronomical Journal* **638** (February 2006).

[6] Give'on, A., Belikov, R., Shaklan, S., and Kasdin, J., "Closed loop, dm diversity based, wave-front correction algorithm for high contrast imaging systems," *Optics Express* **15** (2007).

[7] Guyon, O., Matsuo, T., and Angel, R., "Coronagraphic low-order wave-front sensor : principle and application to a phase-induced amplitude coronagraph," *The Astronomical Journal* **693** (March 2009).

[8] Sauvage, J.-F., Mugnier, L., Paul, B., and Villecroze, R., "Coronagraphic phase diversity: a simple focal plane sensor for high contrast imaging," submitted (2012).

[9] Sauvage, J.-F., Mugnier, L., Rousset, G., and Fusco, T., "Analytical expression of long-exposure adaptative-optics-corrected coronagraphic image. first application to exoplanet detection," *J. Opt. Soc. Am. A.* **27** (November 2010).

[10] Soummer, R., C.Aime, and Falloon, P., "Stellar coronagraphy with prolate apodized circular apertures," *Astron. Astrophys.* **397** (2003).

[11] Roddier, F. and Roddier, C., "Stellar coronagraphy with phase mask," *Astronomical Society of the Pacific* **109** (April 1997).

[12] Guyon, O., Roddier, C., Graves, J., Roddier, F., Cuevas, S., Espejo, C., Gonsalez, S., Martinez, A., Bisiacchi, G., and Vuntesmeri, V., "The nulling stellar coronagraph : laboratory test and performance evaluation," *Astronomical Society of the Pacific* **111** (October 1999).

[13] Soummer, R., L.Pueyo, A.Sivaramakrishnan, and Vanderbei, R., "Fast computation of lyot-style coronagraph propagation," *Optics Express* **15** (November 2007).

[14] Sauvage, J.-F., Fusco, T., Rousset, G., and Petit, C., "Calibration and precompensation of noncommon path aberrations for extrem adaptative optics," *J. Opt. Soc. Am.* **24** (August 2007).

[15] Mugnier, L., C.Robert, Conan, J.-M., Michaud, V., and Salem, S., "Myopic deconvolution from wave-front sensing," *J. Opt. Soc. Am. A* **18** (April 2001).

[16] Thiébault, E. and Conan, J.-M., "Strict a priori constrains for maximum likelihood blind deconvolution," *J. Opt. Soc. Am. A* **12** (March 1995).

[17] Gratadour, D., Mugnier, L., and Rouan, D., "Sub-pixel image registration with a maximum likelihood estimator," *Astron. Astrophys.* **443** (2005).